Nanosecond Optically Induced Phase Transformation in Compressively Strained BiFeO_{3} on LaAlO_{3}

Youngjun Ahn, Anastasios Pateras, Samuel D. Marks, Han Xu, Tao Zhou, Zhenlin Luo, Zuhuang Chen, Lang Chen, Xiaoyi Zhang, Anthony D. DiChiara, Haidan Wen, and Paul G. Evans

Phys. Rev. Lett. **123**, 045703 — Published 26 July 2019
DOI: 10.1103/PhysRevLett.123.045703

Nanosecond Optically Induced Phase Transformation in Compressively Strained $BiFeO_3$ on $LaAlO_3$

Youngjun Ahn,[1] Anastasios Pateras,[1] Samuel D. Marks,[1] Han Xu,[2] Tao Zhou,[3] Zhenlin Luo,[2] Zuhuang Chen,[4] Lang Chen,[5] Xiaoyi Zhang,[6] Anthony D. DiChiara,[6] Haidan Wen,[6] and Paul G. Evans[1,†]

[1] *Department of Materials Science and Engineering, University of Wisconsin-Madison, Madison, Wisconsin 53706, USA*

[2] *National Synchrotron Radiation Laboratory, University of Science and Technology of China, Hefei, Anhui 230026, China*

[3] *ID01/ESRF, 71 Avenue des Martyrs, 38000 Grenoble Cedex, France*

[4] *School of Materials Science and Engineering, Harbin Institute of Technology, Shenzhen 518055, China*

[5] *Department of Physics, Southern University of Science and Technology, Shenzhen, Guangdong 518055, China*

[6] *Advanced Photon Source, Argonne National Laboratory, Argonne, Illinois 60439, USA*

[†] pgevans@wisc.edu

Abstract

Above-bandgap optical illumination of compressively strained $BiFeO_3$ induces a transient reversible transformation from a state of coexisting tilted tetragonal-like and rhombohedral-like phases to an untilted tetragonal-like phase. Time-resolved synchrotron x-ray diffraction reveals that the transformation is induced by an ultrafast optically induced lattice expansion that shifts the relative free energies of the tetragonal-like and rhombohedral-like phases. The transformation proceeds at boundaries between regions of the tetragonal-like phase and regions a mixture of tilted phases, consistent with the motion of a phase boundary. The optically induced transformation demonstrates that there are new optically driven routes towards nanosecond-scale control of phase transformations in ferroelectrics and multiferroics.

Ferroelectric and multiferroic oxides can be transformed between structural phases with different structures and properties by applied pressure, stress, and electric or magnetic fields [1-3]. These systems are particularly sensitive to external stimuli when placed near a phase boundary by lattice-mismatched epitaxial growth or chemical substitution [4-6]. Epitaxial growth on an $LaAlO_3$ (LAO) substrate, for example, places multiferroic $BiFeO_3$ (BFO) near the boundary between rhombohedral-like and tetragonal-like phases that differ significantly in their properties [4]. Both phases have monoclinic symmetry but have different directions and magnitudes of the ferroelectric polarization [7,8]. Furthermore, the magnetism of the tetragonal-like phase exhibits weaker order than the rhombohedral-like phase due to the suppression of the canting of the antiferromagnetic sublattice [9,10]. Differences in the Fe-O bond lengths and Fe-Fe distances also lead to differences in the band structure and in electronic and optical properties of the two phases [11]. Understanding the mechanisms of the transformation and how it can be induced at ultrafast timescales has the potential to lead to the creation of optically tunable and reconfigurable complex oxide electronic and optical materials.

A reversible transformation to the tetragonal-like phase of BFO can be driven by an external electric field [12,13]. Density functional theory studies indicate that the tetragonal-like phase becomes energetically favorable when the lattice is expanded along the out-of-plane direction [14]. Several questions remain regarding the transformation mechanisms, the transformation pathway, and its dynamics. A challenge in studying the transformation using an electric fields is that the time resolution is limited by the charging times of the relatively large thin-film devices and with difficulty in applying high fields in electrically leaky materials [14].

Femtosecond-duration above-bandgap optical pulses generate a transient out-of-plane strain in ferroelectrics and multiferroics, providing a non-contact, ultrafast means to investigate their dynamics. Optical excitation of ferroelectrics and multiferroics generates lattice expansion up to on the order of 1% [15-19]. One mechanism of the expansion arises from screening of surface and interfacial bound charges by excited charge carriers, changing the internal electric field and generating electromechanical distortion [19,20]. Studies of the electrically driven BFO phase transformation indicate that the optically excited expansion would be sufficiently large to induce the transformation to the tetragonal-like phase [14].

Here we report a rapid reversible transformation between phases in compressively strained BFO induced by ultrafast optical excitation. Time-resolved x-ray microdiffraction shows that the optically induced lattice expansion and the transformation both reach their maxima within 1 ns after excitation. X-ray microscopy shows that the transformation occurs in regions in which there are boundaries between the tetragonal-like phase and the tilted tetragonal-like and tilted rhombohedral-like phases. Together, these observations suggest a mechanism in which the tetragonal-like phase is stabilized by the lattice expansion and grows into regions of coexisting populations of the tilted tetragonal-like and tilted rhombohedral-like phases. The structural changes during the optically induced transition are distinct from those at high temperature, including differences in the variation of the lattice parameter and phase population.

Time-resolved x-ray microdiffraction experiments were conducted at station 7ID-C of the Advanced Photon Source using the arrangement in Fig. 1(a). X-rays with a photon energy of 11 keV and 100 ps pulse duration were focused to a 400 nm full-width-at-half-maximum (FWHM) probe spot. The optical pump consisted of 50-fs-duration pulses with 1 kHz repetition rate and 400 nm wavelength, above the bandgap of BFO on LAO [21-23]. A complementary full-field x-ray diffraction microscopy study employed beamline ID-01 of the European Synchrotron Radiation Facility [24].

The 70 nm-thick BFO thin film was grown on an $La_{0.7}Sr_{0.3}MnO_3$ (LSMO) bottom electrode on LAO by pulsed laser deposition [12]. The tetragonal-like and rhombohedral-like phases are referred to as the T and R phases, respectively [4]. The epitaxial mismatch of -4.5% between BFO and LAO leads to the formation of the T phase, the stable form at high compressive strain. The stored elastic energy of the film is reduced by forming regions of stripes of alternating tilted-T (TT) and tilted-R (TR) phases with widths of approximately 50 nm within the larger field of the T phase [4,8,25-27]. Figures 1(b)-(d) show the diffracted intensity near the 002 T phase reflection acquired with an unfocused 50 μm FWHM x-ray beam, averaging over all BFO phases. Figure 1(b) shows part of the Q_z-Q_y plane of reciprocal space in which the TT and TR phases appear at Q_z = 2.69 Å^{-1} and 3.02 Å^{-1}, respectively. Eight intensity maxima arising from the TT phase and a single T reflection appear in the Q_y-Q_x plane at Q_z = 2.70 Å^{-1} in Fig. 1(c). The TR phase also exhibits four pairs of reflections, as in Fig. 1(d). The eight intensity maxima of the TT and TR phases indicate that there are eight domains of each tilted phase [12,28,29]. The reflections in Figs. 1(c) and (d) are numbered in order to discuss them precisely. In the striped microstructure, the TT reflections (1) and (4) are paired with the TR reflections (5) and (8), respectively [27,30,31].

Optical excitation leads to an expansion of the T phase, as in Fig. 1(e), in which the 002 T phase reflection measured using x-ray microdiffraction is shifted to a lower Q_z at 1 ns after excitation at an fluence of 10.7 mJ/cm^2. At this fluence, the lattice expansion has a magnitude of 0.16% and is accompanied by an 8% increase in the integrated diffracted intensity. The changes in the volume of the film occupied by each phase were measured using the changes in the integrated intensities of corresponding x-ray reflections. The phase populations were determined using an analysis considering the different scattering factors of each phase (see Supplemental

Material [32]). The T, TT, and TR phases initially occupy 75%, 15%, and 10% of the film, respectively, matching report for BFO films on LAO with similar thicknesses [4]. The intensities of the TT and TR reflections decreased by 28% and 7%, respectively, at 1 ns with a fluence of 10.7 mJ/cm^2. The population changes indicate that there is a transformation from the TT and TR phases to the T phase.

The variation of the out-of-plane lattice parameter of the T phase as a function of the delay time t is shown in Fig. 2(a) for a fluence of 10.7 mJ/cm^2. The out-of-plane lattice expansion of the T phase was 0.14% at t=200 ps and reached a maximum of 0.16% at t=1 ns. Two physical effects are apparent in the expansion of the T phase. The initial expansion occurs with a timescale set by the propagation of a longitudinal elastic wave through the film thickness, on the order of tens of ps, which is less than the experimental time resolution [17]. A second, long-timescale, component of the lattice expansion, apparent from 200 ps to 1 ns in Fig. 2(a), is not consistent with the acoustic response and is compared below with the timescale of the motion of the phase boundaries. The possibility that thermal diffusion produces the slow risetime can be evaluated by comparing the thermal diffusion length $\sqrt{Dt}$ with the film thickness. Using $D=1.2\times10^{-4}$ m^2/s [19] gives $\sqrt{Dt}$=350 nm at t=1 ns, which is far larger than the BFO thickness and indicates that the peak average temperature is reached at a far shorter time than 1 ns. A complete thermal diffusion simulation based on methods in ref. [39] appears in the Supplementary Material.

The integrated intensity of the T phase reflection, Fig. 2(b), increases for times up to 1 ns. The intensities of the TT (4) and TR (8) reflections decrease after optical excitation and reach minima at time t=1 ns, matching the timescale of the change in the T phase intensity. At t=1 ns, the population of the T phase increases to 81% of the BFO volume, and gradually returns to 76%

at t=12 ns. The populations of the TT and TR phases decrease to 10% and 9% at t=1 ns, respectively, in agreement with the 6% change in the T phase population at that time. In contrast with this mixed-phase sample, optical excitation of pure R phase BFO leads to negligible intensity changes [17-19].

The magnitude of the T phase lattice expansion increases at higher fluence, reaching 0.45% at t=1 ns at 20 mJ/cm^2, as in Fig. 3(a). The intensities of the T, TT, and TR phases also exhibit larger-magnitude changes as a function of increasing fluence, as in Fig. 3(b). The monotonic variation of the intensity changes is consistent with a continuous shift of the energetic balance between the competing phases rather than a transformation at a critical value of the optically induced expansion. A similar continuous transformation with increasing electric field is observed in the electric-field-driven transformation from R to T phases of BFO [14].

A Landau-Ginzburg-Devonshire model was used to predict the energetic stability of the T and R phases as a function of the optically induced distortion. The phases have equal free energies at a biaxial misfit strain of -4.3%, consistent with the previously reported phase boundary. An out-of-plane lattice increases the free energy of the T phase less than the R phase (see Supplementary Material) and favors a transformation from the R phase to the T phase. The difference in the free energies grows monotonically with lattice expansion. The continuous increase in the free-energy difference agrees with the experimental observation that the transformation proceeds without a single threshold value of the fluence or expansion.

The differences between optical excitation and heating were evaluated using variable-temperature diffraction with a laboratory x-ray source. As shown in Fig. 3(c), the T phase lattice parameter expands by 0.45% from room temperature to 110 ºC and shrinks as the temperature increases from 110 ºC to 200 ºC, where it has a value close to the lattice parameter at 90 ºC. The variation of the intensities during heating, Fig. 3(d), does not match the intensity changes resulting from the optically induced transformation. First, heating leads to a decrease (rather than the optically induced increase) in the T phase intensity, by 20% at 110 ºC. A similar intensity decrease has been observed in pure T phase BFO, which indicates that the decrease in the intensity of the T phase reflection at elevated temperatures does not originate from a phase transformation [40]. Similarly, the intensities of the TT and TR phases are not consistent with a transformation between phases below 130 ºC. The change in integrated intensity of the TR phase reflection is negligible during heating to 130 ºC. The TT phase reflection intensity increases by 10% at 70 ºC and drops to its room-temperature value at 130 ºC.

The transformation observed at high temperature is also distinct from the optically induced transformation. From 140 ºC to 200 ºC, the intensities of the TT and TR phase reflections decrease and the intensity of the T phase reflection increases, matching literature reports [25,26]. A key difference between optical and thermal effects, however, is that the high-temperature phase transformation occurs in a regime in which the lattice parameter of the T phase decreases, opposite to the optically excited observation. Similarly, the initial increase in the T phase lattice parameter during heating is accompanied by a decrease in the T phase intensity, rather than the increase observed during optically induced expansion.

The spatial arrangement of the coexisting BFO phases suggests a mechanism for the transformation. Scanning x-ray microdiffraction images reveal that the TT and TR phases exist in multiple spatially separated populations and that the optically induced transformation occurs via the simultaneous changes in the coexisting variants. Microdiffraction maps of the integrated intensities of TT (4) and TR (8) phase reflections, Fig. 4(a), show that these variants occur in the same region, matching previous reports [29]. A similar spatial correlation is also exhibited by the

TT (1) and TR (5) variants and is observed in full-field x-ray microscopy (see Supplementary Material).

A time-resolved microscopy study was conducted to probe the spatial variation of the optically induced transformation. The lattice expansion in the T phase was measured using reciprocal space maps acquired in a 1.2 μm × 200 μm area at the position indicated by arrows in Fig. 4(a) before optical excitation and at t=1 ns following pulses with a fluence of 10.7 mJ/cm^2. The optically induced T-phase lattice expansion in Fig. 4(b) is independent of position, which indicates that the expansion does not depend on the local phase population.

The optically induced change in intensity and the extent of the optically induced transformation depend very strongly on the local phase population. The T phase intensity and the fractional change in intensity after optical excitation both vary significantly as a function of position, as shown in Figs. 4(c) and 4(d). In contrast with the nearly constant optically induced expansion, the fractional change in T phase intensity ranges from 0 to nearly 20%. Regions with near-zero change in the T-phase intensity exhibit two key structural features: (i) these regions have low TT and TR phase population (see Supplemental Material) and (ii) the T phase lattice parameter, Fig. 4(b), is large and has a value close to the lattice parameter of films in which the T phase has not elastically relaxed through the formation of other phases [41]. Taken together, these observations indicate that the transformation proceeds only in regions where T, TT, and TR phases coexist.

The observation here of a simultaneous decrease in TT and TR phase reflections following optical excitation is not consistent with a previously proposed sequential transformation mechanism involving an initial transition between the TR and TT phases, followed by a subsequent transformation to the T phase [31]. The simultaneous and proportional changes in the intensities of x-ray reflections of spatially coexisting tilted phases instead suggest a mechanism in which the tilted phases are simultaneously transformed to the T phase. A mesoscopic process that would enable the simultaneous and continuous transformation from a mixture of TT and TR phases to the T phase is illustrated in Fig. 4(e). In this process, the boundary between the T phase and the TT and TR phases progresses into the mixed phase region. A similar growth of the T phase into mixed-phase regions has been observed using band-excitation piezoelectric force microscopy, with nearly equal magnitudes of the transient T-phase lattice expansion and a transformation over lateral distances consistent with the changes in TT and TR phase populations reported here [42].

The observation of the optically induced transformation in BFO has several implications in understanding and applying phase transformations in ferroelectrics and related materials. With respect to electromechanical distortion, the results suggest that nanosecond-scale lattice expansion with a large contribution arising from the transformation between phases can be produced by optical excitation. Furthermore, the optically induced phase transformation can potentially suppress the magnetic moments of BFO because the transformed part of the film changes from the R phase, which has a large magnetic ordering, to pure T phase with weak magnetic order [10]. This work ultimately broadens the potential of ultrafast optical excitation to change structural phases and coupled multiferroic properties.

This work was supported by the US National Science Foundation through grant number DMR-1609545. H. W. acknowledges the support of U.S. Department of Energy, Office of Science, Basic Energy Sciences, Materials Sciences and Engineering Division, for instrumentation development of time-resolved x-ray microdiffraction. This research used resources of the

Advanced Photon Source, a U.S. Department of Energy Office of Science User Facility operated for the DOE Office of Science by Argonne National Laboratory under Contract No. DE-AC02-06CH11357. Z. H. C. acknowledges the National Science Foundation of China (No. 51802057) and a startup grant from Harbin Institute of Technology, Shenzhen, China, under project number DD45001017. Z. L. Luo and H. Xu were supported by the National Key Basic Research Program of China (2016YFA0300102) and the National Natural Science Foundation of China (11434009, 11675179, U1532142). L. C. acknowledges the Science and Technology Research Items of Shenzhen (JCYJ20170412153325679 and JCYJ20180504165650580).

[1] Z. G. Wu and R. E. Cohen, Phys. Rev. Lett. **95**, 037601 (2005).

[2] P. E. Janolin, B. Dkhil, M. Davis, D. Damjanovic, and N. Setter, Appl. Phys. Lett. **90**, 152907 (2007).

[3] M. Davis, D. Damjanovic, and N. Setter, Phys. Rev. B **73**, 014115 (2006).

[4] R. J. Zeches, M. D. Rossell, J. X. Zhang, A. J. Hatt, Q. He, C. H. Yang, A. Kumar, C. H. Wang, A. Melville, C. Adamo, G. Sheng, Y. H. Chu, J. F. Ihlefeld, R. Erni, C. Ederer, V. Gopalan, L. Q. Chen, D. G. Schlom, N. A. Spaldin, L. W. Martin, and R. Ramesh, Science **326**, 977 (2009).

[5] L. You, P. Caesario, L. Fang, P. Ren, L. Wang, Y. Zhou, A. Gruverman, and J. L. Wang, Phys. Rev. B **90**, 134110 (2014).

[6] P. Sharma, K. R. Kang, Y. Y. Liu, B. K. Jang, J. Y. Li, C. H. Yang, and J. Seidel, Nanotechnology **29**, 205703 (2018).

[7] J. X. Zhang, Q. He, M. Trassin, W. Luo, D. Yi, M. D. Rossell, P. Yu, L. You, C. H. Wang, C. Y. Kuo, J. T. Heron, Z. Hu, R. J. Zeches, H. J. Lin, A. Tanaka, C. T. Chen, L. H. Tjeng, Y. H. Chu, and R. Ramesh, Phys. Rev. Lett. **107**, 147602 (2011).

[8] M. D. Rossell, R. Erni, M. P. Prange, J. C. Idrobo, W. Luo, R. J. Zeches, S. T. Pantelides, and R. Ramesh, Phys. Rev. Lett. **108**, 047601 (2012).

[9] A. J. Hatt, N. A. Spaldin, and C. Ederer, Phys. Rev. B **81**, 054109 (2010).

[10] Q. He, Y. H. Chu, J. T. Heron, S. Y. Yang, W. I. Liang, C. Y. Kuo, H. J. Lin, P. Yu, C. W. Liang, R. J. Zeches, W. C. Kuo, J. Y. Juang, C. T. Chen, E. Arenholz, A. Scholl, and R. Ramesh, Nature Commun. **2**, 225 (2011).

[11] P. Chen, N. J. Podraza, X. S. Xu, A. Melville, E. Vlahos, V. Gopalan, R. Ramesh, D. G.

Schlom, and J. L. Musfeldt, Appl. Phys. Lett. **96**, 131907 (2010).

[12] Z. Chen, Z. Luo, C. Huang, Y. Qi, P. Yang, L. You, C. Hu, T. Wu, J. Wang, C. Gao, T. Sritharan, and L. Chen, Adv. Funct. Mater. **21**, 133 (2011).

[13] L. You, Z. Chen, X. Zou, H. Ding, W. Chen, L. Chen, G. Yuan, and J. Wang, ACS Nano **6**, 5388 (2012).

[14] M. P. Cosgriff, P. Chen, S. S. Lee, H. J. Lee, L. Kuna, K. C. Pitike, L. Louis, W. D. Parker, H. Tajiri, S. M. Nakhmanson, J. Y. Jo, Z. Chen, L. Chen, and P. G. Evans, Adv. Electron. Mater. **2**, 1500204 (2016).

[15] B. Kundys, M. Viret, D. Colson, and D. O. Kundys, Nature Mater. **9**, 803 (2010).

[16] D. Daranciang, M. J. Highland, H. Wen, S. M. Young, N. C. Brandt, H. Y. Hwang, M. Vattilana, M. Nicoul, F. Quirin, J. Goodfellow, T. Qi, I. Grinberg, D. M. Fritz, M. Cammarata, D. Zhu, H. T. Lemke, D. A. Walko, E. M. Dufresne, Y. Li, J. Larsson, D. A. Reis, K. Sokolowski-Tinten, K. A. Nelson, A. M. Rappe, P. H. Fuoss, G. B. Stephenson, and A. M. Lindenberg, Phys. Rev. Lett. **108**, 087601 (2012).

[17] D. Schick, M. Herzog, H. Wen, P. Chen, C. Adamo, P. Gaal, D. G. Schlom, P. G. Evans, Y. Li, and M. Bargheer, Phys. Rev. Lett. **112**, 097602 (2014).

[18] Y. Li, C. Adamo, P. Chen, P. G. Evans, S. M. Nakhmanson, W. Parker, C. E. Rowland, R. D. Schaller, D. G. Schlom, D. A. Walko, H. Wen, and Q. Zhang, Scientific Rep. **5**, 16650 (2015).

[19] H. Wen, P. Chen, M. P. Cosgriff, D. A. Walko, J. H. Lee, C. Adamo, R. D. Schaller, J. F. Ihlefeld, E. M. Dufresne, D. G. Schlom, P. G. Evans, J. W. Freeland, and Y. Li, Phys. Rev. Lett. **110**, 037601 (2013).

[20] Y. Ahn, J. Park, A. Pateras, M. B. Rich, Q. Zhang, P. Chen, M. H. Yusuf, H. Wen, M.

Dawber, and P. G. Evans, Phys. Rev. Lett. **119**, 057601 (2017).

[21] H. L. Liu, M. K. Lin, Y. R. Cai, C. K. Tung, and Y. H. Chu, Appl. Phys. Lett. **103**, 181907 (2013).

[22] C. Himcinschi, A. Bhatnagar, A. Talkenberger, M. Barchuk, D. R. T. Zahn, D. Rafaja, J. Kortus, and M. Alexe, Appl. Phys. Lett. **106**, 012908 (2015).

[23] D. Sando, Y. Yang, E. Bousquet, C. Carretero, V. Garcia, S. Fusil, D. Dolfi, A. Barthelemy, P. Ghosez, L. Bellaiche, and M. Bibes, Nature Commun. **7**, 10718 (2016).

[24] J. Hilhorst, F. Marschall, T. N. Tran Thi, A. Last, and T. U. Schülli, J. Appl. Cryst. **47**, 1882 (2014).

[25] A. R. Damodaran, S. Lee, J. Karthik, S. MacLaren, and L. W. Martin, Phys. Rev. B **85**, 024113 (2012).

[26] H.-J. Liu, C.-W. Liang, W.-I. Liang, H.-J. Chen, J.-C. Yang, C.-Y. Peng, G.-F. Wang, F.-N. Chu, Y.-C. Chen, H.-Y. Lee, L. Chang, S.-J. Lin, and Y.-H. Chu, Phys. Rev. B **85**, 014104 (2012).

[27] C. Beekman, W. Siemons, T. Z. Ward, M. Chi, J. Howe, M. D. Biegalski, N. Balke, P. Maksymovych, A. K. Farrar, J. B. Romero, P. Gao, X. Q. Pan, D. A. Tenne, and H. M. Christen, Adv. Mater. **25**, 5561 (2013).

[28] Z. Chen, S. Prosandeev, Z. L. Luo, W. Ren, Y. Qi, C. W. Huang, L. You, C. Gao, I. A. Kornev, T. Wu, J. Wang, P. Yang, T. Sritharan, L. Bellaiche, and L. Chen, Phys. Rev. B **84**, 094116 (2011).

[29] Z. Chen, Z. Luo, Y. Qi, P. Yang, S. Wu, C. Huang, T. Wu, J. Wang, C. Gao, T. Sritharan, and L. Chen, Appl. Phys. Lett. **97**, 242903 (2010).

[30] Z. L. Luo, H. Huang, H. Zhou, Z. H. Chen, Y. Yang, L. Wu, C. Zhu, H. Wang, M. Yang, S. Hu, H. Wen, X. Zhang, Z. Zhang, L. Chen, D. D. Fong, and C. Gao, Appl. Phys. Lett. **104**, 182901 (2014).

[31] A. R. Damodaran, C. W. Liang, Q. He, C. Y. Peng, L. Chang, Y. H. Chu, and L. W. Martin, Adv. Mater. **23**, 3170 (2011).

[32] See Supplemental Material, which includes Refs. [33-38], at [url] for more detailed discussion of the experimental setup, data analysis and theoretical calculations.

[33] F. Kubel and H. Schmid, Acta Cryst. **B46**, 698 (1990).

[34] N. A. Pertsev, A. G. Zembilgotov, and A. K. Tagantsev, Phys. Rev. Lett. **80**, 1988 (1998).

[35] V. G. Koukhar, N. A. Pertsev, and R. Waser, Phys. Rev. B **64**, 214103 (2001).

[36] Y. Y. Liu, L. Yang, and J. Y. Li, J. Appl. Phys. **113**, 183524 (2013).

[37] R. B. Wilson, B. A. Apgar, W.-P. Hsieh, L. W. Martin, and D. G. Cahill, Phys. Rev. B **91**, 115414 (2015).

[38] W. Schnelle, R. Fischer, and E. Gmelin, J. Phys. D: Appl. Phys. **34**, 846 (2001).

[39] D. A. Walko, Y. M. Sheu, M. Trigo, and D. A. Reis, J. Appl. Phys. **110**, 102203 (2011).

[40] K. T. Ko, M. H. Jung, Q. He, J. H. Lee, C. S. Woo, K. Chu, J. Seidel, B. G. Jeon, Y. S. Oh, K. H. Kim, W. I. Liang, H. J. Chen, Y. H. Chu, Y. H. Jeong, R. Ramesh, J. H. Park, and C. H. Yang, Nature Commun. **2**, 567 (2011).

[41] H. Bea, B. Dupe, S. Fusil, R. Mattana, E. Jacquet, B. Warot-Fonrose, F. Wilhelm, A. Rogalev, S. Petit, V. Cros, A. Anane, F. Petroff, K. Bouzehouane, G. Geneste, B. Dkhil, S. Lisenkov, I. Ponomareva, L. Bellaiche, M. Bibes, and A. Barthelemy, Phys. Rev. Lett. **102**,

217603 (2009).

[42] R. K. Vasudevan, M. B. Okatan, Y. Y. Liu, S. Jesse, J.-C. Yang, W.-I. Liang, Y.-H. Chu, J. Y. Li, S. V. Kalinin, and V. Nagarajan, Phys. Rev. B **88**, 020402 (2013).

FIG 1. (a) X-ray diffraction experimental schematic illustrating the directions of the optical and x-ray pulses and the mesoscale arrangement of coexistenting TT, TR, and T phases. Arrows illustrate the growth of the T phase region by phase boundary motion. (b) Section of the Q_y-Q_z plane of reciprocal space at Q_x = 0, near the 002 T phase reflection. (c) TT and T phase reflections in the Q_x-Q_y plane at Q_z = 2.70 Å^{-1}. (d) TR phase reflections in the Q_x-Q_y plane, integrating from Q_z =2.90 Å^{-1} to 3.08 Å^{-1}. Individual reflections are numbered. (e) Intensity as a function of Q_z for the 002 T phase reflection before optical excitation and at t=1 ns with fluence 10.7 mJ/cm^2.

FIG 2. (a) Lattice expansion in the T phase and (b) fractional intensity changes of T, TR (8), and TT (4) phase reflections as a function of time following optical excitation at fluence 10.7 mJ/cm^2.

FIG 3. (a) T phase lattice expansion and (b) integrated intensities of the T, TT (1), TT (4), TR (5) and TR (8) reflections as a function of fluence at t=1 ns. Angular scans recording the intensities were conducted for different numbers of values of the fluence for each phase, resulting in different numbers of fluence points for each reflection. (c) T phase lattice expansion and (d) integrated intensities of the T, TT, and TR phase reflections as a function of temperature.

FIG 4. (a) Scanning x-ray microdiffraction maps of TT (4) and TR (8) phases. (b) Lattice expansion along the out-of-plane direction, out-of-plane lattice parameters, (c) integrated intensities before optical excitation and at t=1 ns, and (d) fractional T phase intensity change along the line indicated by black arrows in (a). Shaded areas in (c) and (d) indicate regions with large T phase lattice parameter and small changes in the T phase population. (e) Top-view schematic of an optically induced phase transformation mechanism involving expansion of the T phase into the region of mixed TT and TR phases.

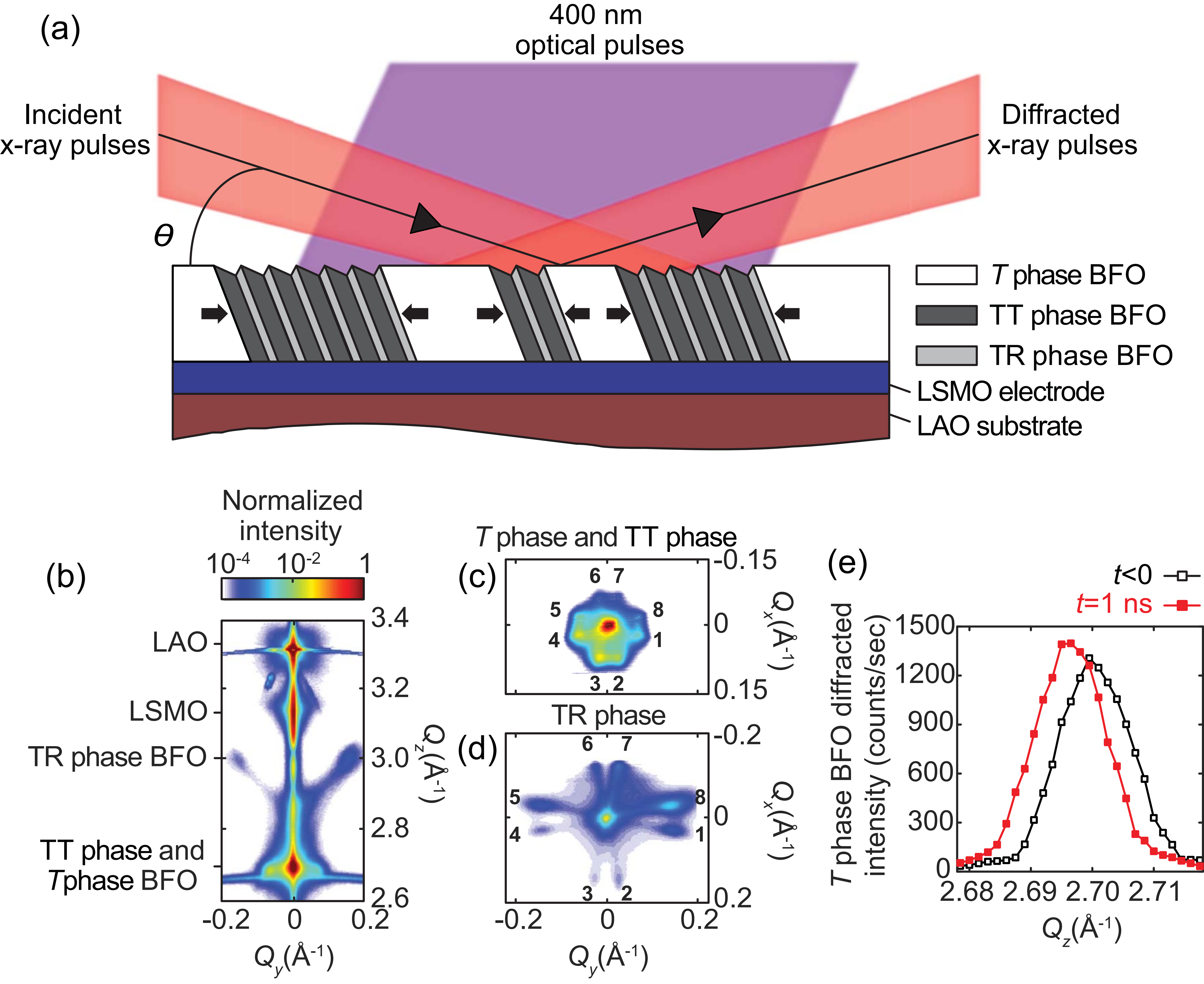
(a)
400 nm
optical pulses
Incident
x-ray pulses
Diffracted
x-ray pulses
θ
T phase BFO
TT phase BFO
TR phase BFO
LSMO electrode
LAO substrate
(b)
Normalized
intensity
10^-4
10^-2
1
LAO
LSMO
TR phase BFO
TT phase and
T phase BFO
3.4
3.2
3.0
2.8
2.6
Q_z(Å^-1)
-0.2
0
0.2
Q_y(Å^-1)
T phase and TT phase
(c)
6 7
5
8
4
1
3 2
-0.15
0
0.15
Q_x(Å^-1)
TR phase
(d)
6 7
5
8
4
1
3 2
-0.2
0
0.2
Q_x(Å^-1)
-0.2
0
0.2
Q_y(Å^-1)
(e)
t<0
t=1 ns
T phase BFO diffracted
intensity (counts/sec)
1500
1200
900
600
300
0
2.68
2.69
2.70
2.71
Q_z(Å^-1)

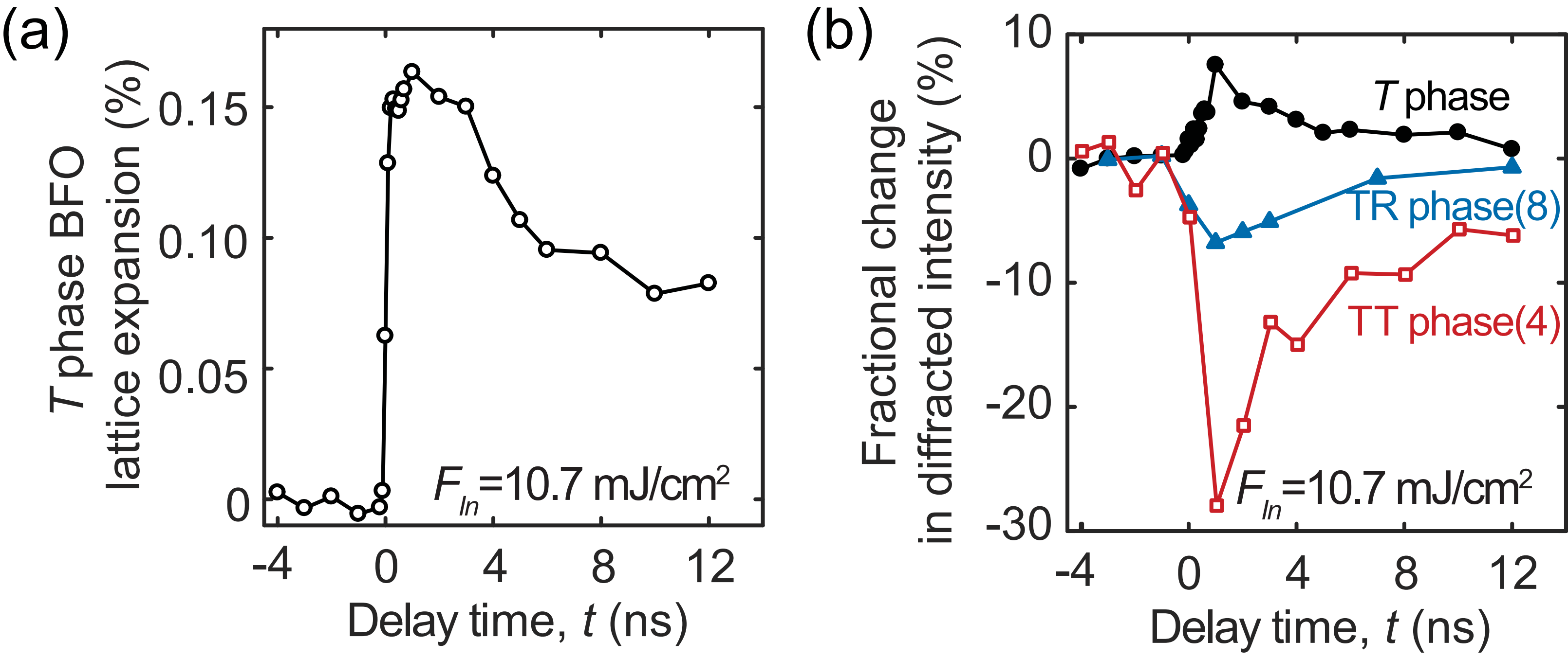
(a)
T phase BFO lattice expansion (%)
0.15
0.10
0.05
0
-4
0
4
8
12
Delay time, t (ns)
F_{In}=10.7 mJ/cm^2
(b)
Fractional change in diffracted intensity (%)
10
0
-10
-20
-30
-4
0
4
8
12
Delay time, t (ns)
T phase
TR phase(8)
TT phase(4)
F_{In}=10.7 mJ/cm^2

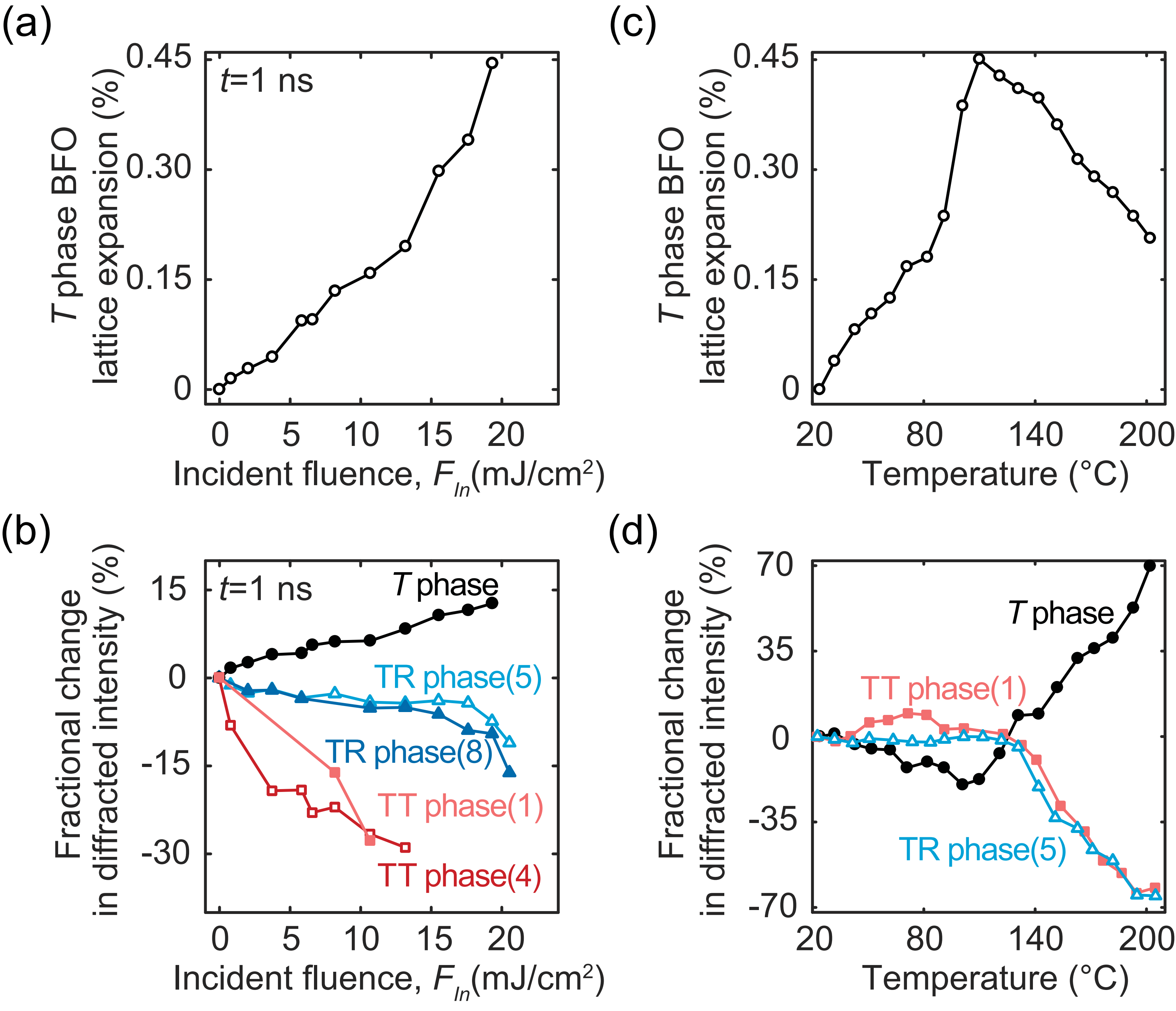
(a)
t=1 ns
T phase BFO lattice expansion (%)
0.45
0.30
0.15
0
0
5
10
15
20
Incident fluence, F_{In}(mJ/cm^2)
(b)
t=1 ns
Fractional change in diffracted intensity (%)
15
0
-15
-30
T phase
TR phase(5)
TR phase(8)
TT phase(1)
TT phase(4)
0
5
10
15
20
Incident fluence, F_{In}(mJ/cm^2)
(c)
T phase BFO lattice expansion (%)
0.45
0.30
0.15
0
20
80
140
200
Temperature (°C)
(d)
Fractional change in diffracted intensity (%)
70
35
0
-35
-70
T phase
TT phase(1)
TR phase(5)
20
80
140
200
Temperature (°C)

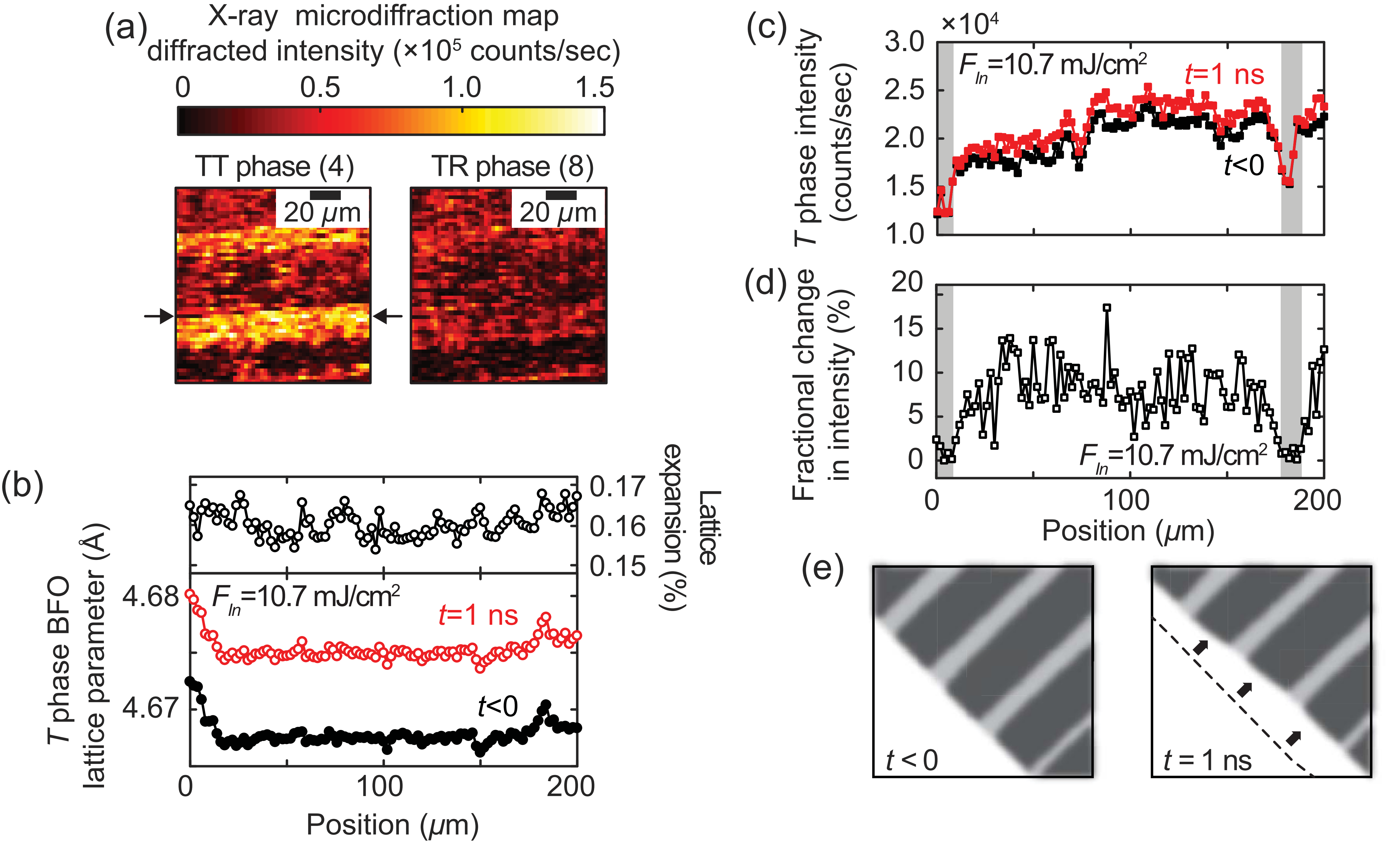
(a)
X-ray microdiffraction map
diffracted intensity (×10⁵ counts/sec)
0
0.5
1.0
1.5
TT phase (4)
TR phase (8)
20 μm
20 μm
(b)
T phase BFO lattice parameter (Å)
Lattice expansion (%)
0.17
0.16
0.15
4.68
4.67
F_In=10.7 mJ/cm²
t=1 ns
t<0
0
100
200
Position (μm)
(c)
T phase intensity (counts/sec)
×10⁴
3.0
2.5
2.0
1.5
1.0
F_In=10.7 mJ/cm²
t=1 ns
t<0
(d)
Fractional change in intensity (%)
20
15
10
5
0
F_In=10.7 mJ/cm²
0
100
200
Position (μm)
(e)
t < 0
t = 1 ns